ISSN 1674-1056
http://cpb.iphy.ac.cn
http://iopscience.iop.org/cpb
中国物理 B
Chinese Physics
中国物理
Chinese Physics B

High capacity sodium-rich layered oxide cathode for sodium-ion batteries

Gen-Cai Guo(郭根材), Changhao Wang(王长昊), Bang-Ming Ming(明帮铭), Si-Wei Luo(罗斯玮), Heng Su(苏恒), Bo-Ya Wang(王博亚), Ming Zhang(张铭), Hai-Jun Yu(尉海军), Ru-Zhi Wang(王如志)

Citation: Chin. Phys. B . 2018, 27(11): 118801. **doi:** 10.1088/1674-1056/27/118801
Journal homepage: http://cpb.iphy.ac.cn; http://iopscience.iop.org/cpb

What follows is a list of articles you may be interested in

First principles study of stability, mechanical, and electronic properties of chromium silicides

Bo Ren(任博), De-Hong Lu(卢德宏), Rong Zhou(周荣), De-Peng Ji(姬德朋), Ming-Yu Hu(胡明钰), Jing Feng(冯晶)
Chin. Phys. B . 2018, 27(10): 107102. **doi:** 10.1088/1674-1056/27/10/107102

Multiscale energy density algorithm and application to surface structure of Ni matrix of superalloy

Min Sun(孙敏), Chong-Yu Wang(王崇愚), Ji-Ping Liu(刘吉平)
Chin. Phys. B . 2018, 27(9): 097105. **doi:** 10.1088/1674-1056/27/9/097105

Theoretical study on the kesterite solar cells based on $Cu_2ZnSn(S,Se)_4$ and related photovoltaic semiconductors

Dingrong Liu(刘定荣), Dan Han(韩丹), Menglin Huang(黄梦麟), Xian Zhang(张弦), Tao Zhang(张涛), Chenmin Dai(戴称民), Shiyou Chen(陈时友)
Chin. Phys. B . 2018, 27(1): 018806. **doi:** 10.1088/1674-1056/27/1/018806

All-solid-state lithium batteries with inorganic solid electrolytes: Review of fundamental science

Xiayin Yao(姚霞银), Bingxin Huang(黄冰心), Jingyun Yin(尹景云), Gang Peng(彭刚), Zhen Huang(黄祯), Chao Gao(高超), Deng Liu(刘登), Xiaoxiong Xu(许晓雄)
Chin. Phys. B . 2016, 25(1): 018802. **doi:** 10.1088/1674-1056/25/1/018802

Scientific and technological challenges toward application of lithium-sulfur batteries

Ya-Xia Yin(殷雅侠), Hu-Rong Yao(姚胡蓉), Yu-Guo Guo(郭玉国)
Chin. Phys. B . 2016, 25(1): 018801. **doi:** 10.1088/1674-1056/25/1/018801

High capacity sodium-rich layered oxide cathode for sodium-ion batteries*

Gen-Cai Guo(郭根材), Changhao Wang(王长昊), Bang-Ming Ming(明帮铭), Si-Wei Luo(罗斯玮), Heng Su(苏恒), Bo-Ya Wang(王博亚), Ming Zhang(张铭), Hai-Jun Yu(尉海军)†, and Ru-Zhi Wang(王如志)‡

College of Materials Science and Engineering, Beijing University of Technology, Beijing 100124, *China*

(Received 29 July 2018; revised manuscript received 4 September 2018; published online 24 October 2018)

Sodium-ion batteries have attracted significant recent attention currently considering the limited available lithium resource. However, the energy density of sodium-ion batteries is still insufficient compared to lithium-ion batteries, mainly because of the unavailability of high-energy cathode materials. In this work, a novel sodium-rich layered oxide material (Na_2MnO_3) is reported with a dynamical stability similar to that of the Li_2MnO_3 structure and a high capacity of 269.69 mA·h·g^1, based on first-principles calculations. Sodium ion de-intercalation and anionic reaction processes are systematically investigated, in association with sodium ions migration phenomenon and structure stability during cycling of Na_xMnO_3 ($1 \leq x \leq 2$). In addition, the charge compensation during the initial charging process is mainly contributed by oxygen, where the small differences of the energy barriers of the paths 2c→4h, 4h→2c, 4h→4h, 2c→2b, and 4h→2b indicate the reversible sodium ion occupancy in transitional metal and sodium layers. Moreover, the slow decrease of the elastic constants is a clear indication of the high cycle stability. These results provide a framework to exploit the potential of sodium-rich layered oxide, which may facilitate the development of high-performance electrode materials for sodium-ion batteries.

Keywords: sodium-rich layered oxides, first-principles calculations, sodium-ion diffusion

PACS: 88.80.ff, 71.15.Mb, 71.15.Nc, 71.20.Dg **DOI:** 10.1088/1674-1056/27/11/118801

1. Introduction

The rapid development of intelligent and portable electronic devices has been facilitated by a series of significant breakthroughs in electrode material research in recent years. Due in part to their high-energy density, high capacity and favorable cycle life, lithium-ion batteries (LIBs) have been applied to a wide variety of electronic devices.[1–8] However, the limited and unbalanced distribution of lithium resources along with an increasing industry demand, could result in a lithium shortage crisis in the near future.[9,10] In an attempt to identify novel alternative materials, room temperature sodium-ion batteries (NIBs) are considered as promising candidates for the next generation of ion batteries and has attracted notable attention due to the abundance of sodium resources, low cost and similar chemical intercalation mechanism compared to LIBs.[11–16]

Currently, the fundamental requirement of electrode materials for NIBs is to address to problem of their limited energy density, which primarily depends on positive active materials.[17] Previously, various compounds, including Na_xCoO_2,[18,19] Na_xMnO_2,[20,21] $NaCrO_2$,[22] $Na_xFe_{0.5}Mn_{0.5}O_2$,[23,24] $NaNi_{0.5}Mn_{0.5}O_2$,[25] $NaNi_{0.5}Ti_{0.5}O_2$,[26] $Na_3MPO_4CO_3$,[27] $NaNi_{1/3}Mn_{1/3}Fe_{1/3}O_2$,[28] $Na_{0.9}Cu_{0.25}Fe_{0.25}Mn_{0.25}Ti_{0.25}O_2$,[29] and $Na_3V_2(PO_4)_3$/rGO,[30] have been investigated as cathode material for NIBs. However, all of these materials have relatively low energy densities and, therefore, it would be difficult for them to achieve broad market penetration. Consequently, there is an existing urgent need to identify a high capacity cathode material for NIBs.

In the development of high capacity NIBs, some existing LIBs cathode materials have important characteristics that are useful for novel material designs. Recently, Li-rich layered oxide (LLO) cathodes have attracted the attention of many researchers due to their high-energy density, where the excess energy is determined by the "Li_2MnO_3" structural component and the anionic reaction contribution.[31–35] Therefore, it is natural to consider whether sodium-rich layered oxides (SLOs) cathode materials with a higher capacity than conventional NIBs cathode materials exist. In the family of LLOs, a layered $Li_2MnO_3LiTMO_2$ (TM = transitional metals) composite has demonstrated exceptional performance with a high capacity of up to 400 mA·h·g^1.[36–38] In these materials, the Li_2MnO_3 structure component plays an important role in reversible capacity.[39] Thus, it can be deduced that there exists a SLOs cathode material, Na_2MnO_3, that presents similar sodium storage properties such as lithium in Li_2MnO_3. Moreover, many researchers have determined that anions such as

*Project suppoted by the National Natural Science Foundation of China (Grant Nos. 11774017, 51761135129, and 51472010) and Beijing Municipal High Level Innovative Team Building Program, China (Grant No. IDHT20170502).

†Corresponding author. E-mail: hj-yu@bjut.edu.cn

‡Corresponding author. E-mail: wrz@bjut.edu.cn

© 2018 Chinese Physical Society and IOP Publishing Ltd

oxygen ions in LLOs are oxidized during Li de-intercalation and that this process resulted in a deterioration of the cycle stability.[33,34,40] For Na_2MnO_3, we also intend to evaluate the structural stability and the intrinsic sodium storage mechanism, which is of significance for the development of SLO cathodes. Recently, Ouyang *et al.* investigated the electronic structures and the migration of Na in Na_2MnO_3.[41] However, the stability, capacity, and cycle performance of Na_2MnO_3 has not been explored. In addition, the mechanism of Na ions in de-intercalation and the corresponding charge compensation are still not clear.

In this work, systematic investigations of the layered Na_2MnO_3 material were performed using a theoretical simulation scheme based on first-principle calculations. It is determined that the Na_2MnO_3 has a high capacity of 269.69 $mA{\cdot}h{\cdot}g^{-1}$ with a similar crystalline structure to Li_2MnO_3. Moreover, the structure and stability of Na_2MnO_3 in addition to the anionic reaction process and the diffusion of Na^+ in Na_2MnO_3 along different paths are examined and discussed in detail. The elastic constants of Na_xMnO_3 ($1 \leq x \leq 2$) are also investigated. These results demonstrate that Na_2MnO_3 is a potential sodium-rich layered oxide material. Our theoretical studies improve the possibility of identifying high capacity NIBs cathode materials, and will likely guide future experimental research work.

2. Computational methods

All of the calculations were performed based on density functional theory (DFT) as implemented in the Vienna ab initio simulation package (VASP).[42] The Perdew–Burke–Ernzerhof approach of spin-polarized generalized gradient approximation (GGAPBE) was used to describe the exchange–correlation energy.[43] Gpoint sampling was used for the integration of the Brillouin zone. The Na(3s), Mn(3d, 4s), and O(2s, 2p) orbitals are treated as valence states. The strong correlation effect of transition metals was addressed using an onsite Hubbard parameter correction for the density functional theory ($U_{Mn} = 3.9$ eV).[44] An energy cutoff of 520 eV was applied in all calculations for the plane-wave expansion of the electronic eigenfunctions. To minimize the effect of periodic boundaries, two supercells with $2 \times 1 \times 1$ (containing 16 sodium atoms, 8 manganese atoms, and 24 oxygen atoms) and $2 \times 1 \times 2$ (contains 32 sodium atoms, 16 manganese atoms, and 48 oxygen atoms) were used to investigate Na^+ de-intercalation and Na^+ migration, respectively. Both the ions and cells are fully relaxed in all of the calculations with the energy and force convergence criterion of 10^5 eV and 0.01 eV/Å, respectively. The phonon spectrums were calculated using PHONONPY code.[45] To understand the kinetics of the mechanism of Na^+ migration, an activation energy barrier was explored using the climbing image nudged elastic band (CINEB) method.[46] In addition, the change of charge distribution was analyzed for the process of Na^+ de-intercalation from the Na_2MnO_3 system by employing a grid-based Bader analysis algorithm.[47]

To investigate the crystalline stability of Na_2MnO_3, the cohesive energy was also calculated, which is defined as[48]

$$E_c = \frac{E_{Na_2MnO_3} - 2E_{Na} - E_{Mn} - 3E_O}{n}, \quad (1)$$

where n is the total number of atoms in the Na_2MnO_3 system. $E_{Na_2MnO_3}$, E_{Na}, E_{Mn}, and E_O are the total energies of the Na_2MnO_3, isolated Na atom, Mn atom, and O atom, respectively. The theoretical capacity is given by

$$C = \frac{1000yN_Ae}{3600M_{Na_2MnO_3}}, \quad (2)$$

where y is the number of Na^+ de-intercalation ($Na_{2y}MnO_3$); N_A is the Avogadro constant; e is the elementary charge; $M_{Na_2MnO_3}$ is the molar mass of Na_2MnO_3. The voltage, V, can be determined by[49]

$$V = \frac{E_{Na_{x_1}MnO_3} - E_{Na_{x_2}MnO_3} - (x_1 - x_2)E_{Na}}{x_1 - x_2}, \quad (3)$$

where x_1 and x_2 represent two variable Na concentrations in the range from 2 to 0; $E_{Na_{x_1}MnO_3}$, $E_{Na_{x_2}MnO_3}$, and E_{Na} are the total energy of $Na_{x_1}MnO_3$, $Na_{x_2}MnO_3$, and metal Na, respectively.

3. Results and discussion

3.1. Stability of Na_2MnO_3

The structure of Na_2MnO_3 was directly constructed by replacing the Li atoms with Na atoms in the Li_2MnO_3 structure. Then, a full geometry optimization for the structure of Na_2MnO_3 was performed. The results indicate that Na_2MnO_3 has a similar arrangement of atoms in Li_2MnO_3, where both the Na^+ and Mn^{4+} ions reside in the octahedral sites of a cubic close-packed, O_3 oxygen lattice. As shown in Fig. 1(a), the manganese layers and the Na layers stack into the $C2/m$ structure and the Na_2MnO_3 can be described as $\{(Na_{1/2})_{2c}(Na)_{4h}\}_{Na-layer}$ $\{(Na_{1/2})_{2b}(Mn)_{4g}\}_{TM-layer}$ $(O)_{4i}(O_2)_{8j}$. Similar to Li^+ in Li_2MnO_3, Na^+ has three occupied sites in Na_2MnO_3, with the 4h and 2c sites in the Na layer and the 2b site in the Mn layer. In this case, the calculated lattice parameters and band gaps of Li_2MnO_3 (in Okamoto's work),[50] Li_2MnO_3 (in this work), and Na_2MnO_3 (in this work) are shown in Table 1. The calculated results for Li_2MnO_3 are very close to those in Ref. [50], indicating that the calculations in this work are reliable and comparable to the previous results. The results indicate that the lattice parameters of Na_2MnO_3 are slightly larger than those of Li_2MnO_3, which is reasonable given that the larger Na atom radius occupies more space in the cell. A superior electrical conductivity of Na_2MnO_3 can be expected

as a result of smaller band gap of Na_2MnO_3 compared to that of Li_2MnO_3.

Table 1. Calculated lattice parameters and band gaps (E_g) of Li_2MnO_3 (in Ref. [50]), Li_2MnO_3 (in this work), and Na_2MnO_3 (in this work).

	Space group	a/Å	b/Å	c/Å	E_g/eV
Li_2MnO_3 [50]	$C2/m$	4.98	8.63	5.00	1.90
Li_2MnO_3	$C2/m$	4.99	8.63	5.07	1.87
Na_2MnO_3	$C2/m$	5.26	9.12	5.63	1.55

The crystalline stability of a proposed material is of vital importance in the evaluation of its difficulty of experimental synthesis and potential application prospects. The cohesive energy of Na_2MnO_3 is calculated as 5.23 eV/atom. Such a large cohesive energy indicates that Na_2MnO_3 is energetically stable. In addition, the thermodynamic stability of Na_2MnO_3 is investigated using *ab-initio* molecular dynamic (AIMD) simulations that adopt NVT canonical ensembles (at a temperature of 800 K). The time step is set to be 1 fs and the total simulation time is more than 10 ps to ensure that the stability conclusions are reliable. The calculated results indicate that the structure of Na_2MnO_3 still maintains the initial state long after AIMD processing, as presented in Fig. 1(b). These results indicate that Na_2MnO_3 is also thermally stable at high temperatures. In order to further evaluate the stability of Na_2MnO_3, phonon spectrum calculations were performed. Based on the results shown in Fig. 1(c), Na_2MnO_3 is confirmed as a dynamically stable structure without any imaginary frequencies. When combined, these results confirm the crystalline stability of Na_2MnO_3.

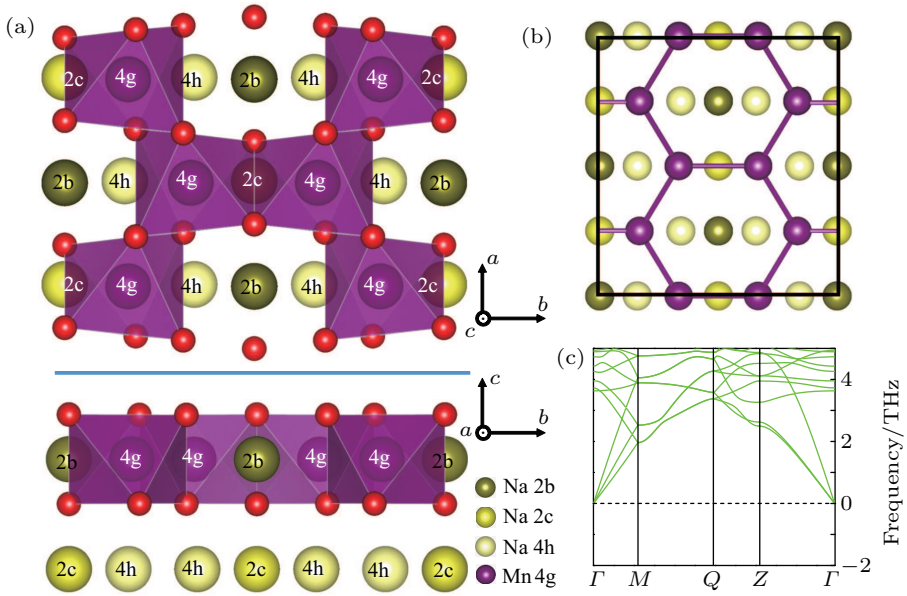


Fig. 1. (color online) (a) Top (upper left) and side (lower left) view of Na_2MnO_3 structure. (b) The structure of Na_2MnO_3 after AIMD simulation. (c) Phonon spectrum of Na_2MnO_3.

3.2. The process of Na^+ de-intercalation from Na_2MnO_3

It is necessary to specify the process of Na^+ de-intercalation in the simulation of electrochemical performance, which is the bottleneck step in the analysis of the mechanism of an electrochemical reaction. In the charging process, Na^+ is continuously extracted from Na_2MnO_3. The ground states of four structures with different concentrations of sodium—i.e., $Na_{1.75}MnO_3$, $Na_{1.5}MnO_3$, $Na_{1.25}MnO_3$, and Na_1MnO_3—were considered. There are 10, 10, 9, and 9 possible configurations for $Na_{1.75}MnO_3$, $Na_{1.5}MnO_3$, $Na_{1.25}MnO_3$, and Na_1MnO_3, respectively, and these structures and their corresponding total energies are shown in Fig. S1–S4. In this case, the four ground-state configurations are selected and depicted in Fig. 2. Initially, Na^+ was extracted from Na_2MnO_3 and subsequently, half of the ions was lost at the 2c site to become $Na_{1.75}MnO_3$, which is represented as the ground state of this compound in Fig. 2. In the case of $Na_{1.5}MnO_3$, all the Na^+ at the 2c site was extracted, and the Na^+ at the 4h site and the 2b site remained. Next, from $Na_{1.5}MnO_3$ to $Na_{1.25}MnO_3$, Na^+ at the 2b site in the Mn layer were extracted and half of them will be removed. Subsequently, all the Na^+ at the 2b site were continually extracted to the $NaMnO_3$.

When the Na^+ concentration of Na_xMnO_3 was equal to that of the Na_1MnO_3 ($x = 1.0$), Na^+ only remained at the 4h site. Throughout the entire charging process from Na_2MnO_3 to $NaMnO_3$, the framework of the layered structure was well maintained except for small changes in the lattice parameters (as shown in Table 2) and the Na/Mn ordering disruption of the Mn layer. Next, we also considered the further extraction of Na^+ (4h site). The calculated results indicate that half of the Na^+ at the 4h site can be extracted and the crystal framework maintains its stability to reach the low Na concentration structure of $Na_{0.5}MnO_3$, for which the ground state configuration is shown in Fig. S5. From Na_2MnO_3 to $Na_{0.5}MnO_3$, the Na^+ de-intercalation capacity can achieve a

value of 269.69 mA·h·g^{-1} which represents a significantly high capacity, calculated using Eq. (2). The cycle voltage between Na_2MnO_3 and $Na_{0.5}MnO_3$ was also calculated, which is in the range of 3.42–4.30 V as obtained from Eq. (3). It should be noted that all of the configurations of $Na_{0.75}MnO_3$, represented as intermediate structures between Na_1MnO_3 to $Na_{0.5}MnO_3$, will deform. Moreover, the stacking sequence of the layered structure will be transferred from O_3 to O_1 when the concentration is lower than that of $Na_{0.5}MnO_3$. This phenomenon is also observed in the Li de-intercalation process of Li_2MnO_3.[51] Considering the potential structural instability of low Na^+ concentrations ($x < 1.0$), we only investigate the Na_xMnO_3 ($1 \leq x \leq 2$) structures, in which excellent reversible intercalation/de-intercalation of Na^+ can be expected without phase transition.

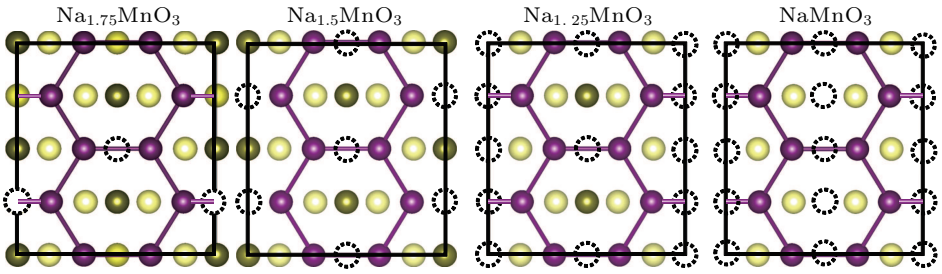


Fig. 2. (color online) Ground-state configuration of $Na_{1.75}MnO_3$, $Na_{1.5}MnO_3$, $Na_{1.25}MnO_3$, and $NaMnO_3$.

Table 2. Lattice parameters of Na_xMnO_3 supercell and the average charge transfer of sodium, manganese, and oxygen, respectively.

Value x in Na_xMnO_3	Distribution of Na^+	Lattice parameter/Å			Average badercharge/e		
		a	b	c	Na	Mn	O
2.00	$\{2c\}_{1/2}\{4h\}_1\{2b\}_{1/2}$	10.52	9.12	5.63	+0.78	+1.74	–1.10
1.75	$\{2c\}_{1/4}\{4h\}_1\{2b\}_{1/2}$	10.32	9.13	5.70	+0.79	+1.74	–1.04
1.50	$\{2c\}_0\{4h\}_1\{2b\}_{1/2}$	10.18	9.10	5.70	+0.79	+1.74	–0.98
1.25	$\{2c\}_0\{4h\}_1\{2b\}_{1/4}$	10.01	9.01	5.64	+0.80	+1.76	–0.92
1.00	$\{2c\}_0\{4h\}_1\{2b\}_0$	9.80	8.92	5.59	+0.80	+1.78	–0.86

3.3. Charge compensation of Na^+ de-intercalation in Na_xMnO_3

Next, the charge compensation mechanism of Na_xMnO_3 ($1 \leq x \leq 2$) was investigated during the charging process via Bader atomic charge analysis. The calculated results are listed in Table 2 and the values of the transferred charge are obtained by subtracting the values of the valence electrons from the calculated charge. The charge of Na^+ for $x = 2.0$ to 1.0 exhibited a negligible difference of +0.78e to +0.80e, and the charge of Mn also exhibited a small difference of +1.74e to +1.78e. These results suggest that the Mn atoms are not oxidized in the process of Na^+ de-intercalation. However, the charge of the O atoms change from −1.10e to −0.86e with a change in x from 2.0 to 1.0. This indicates that charge compensation for Na^+ removal is mainly contributed by the oxidation of O. A similar charge compensation mechanism is also found in the Li de-intercalation process in Li_2MnO_3.[39] In addition, the charge of the O atom surrounding the Na_2MnO_3 has a small fluctuation in the range of $-1.09\,e \sim -1.11e$, which indicates that the MnO_6 octahedron is faultless in Na_2MnO_3. However, in $Na_{1.75}MnO_3$ the charge of the O atom has a larger range of $-1.00\,e \sim -1.10e$ depending on its neighboring environment. Near the vacancy, the charge of the O atom is approximate −1.00e, which is the largest charge value compared with other O atoms. These results indicate that the O atom near the vacancy is responsible for charge compensation during charging in $Na_{1.75}MnO_3$. Similar situations of unbalanced charge distributions are also found in other configurations of Na_xMnO_3 ($x = 1.5$, 1.25, and 1.0).

To further evaluate the phenomenon of charge compensation, the partial densities of states (PDOS) for Na_xMnO_3 ($x = 2.0$, 1.75, 1.5, 1.25, and 1.0) were calculated. Figure 3 shows that the densities of states near the Fermi level are mainly attributable to the 2p orbits of the O atom and partially to the 3d orbits of Mn. With the removal of Na^+, an increasing number of holes in the 2p states of O are formed, therefore, the Fermi level moves in the low energy direction as depicted in Figs. 3(a)–3(e). Meanwhile, it should be noted that the charge compensation of the 2p orbit of O is much larger than that of the 3d orbit of Mn, due to the larger density of states contributions of the O atoms near the Fermi level. In this case, the charge compensations mainly occur in the O atoms near the vacated Na during the Na^+ de-intercalation process, which is consistent with the previous results from the Bader atomic charge analysis. This charge compensation mechanism is very similar to that presented in a previous investigation on Li_2MnO_3.[39]

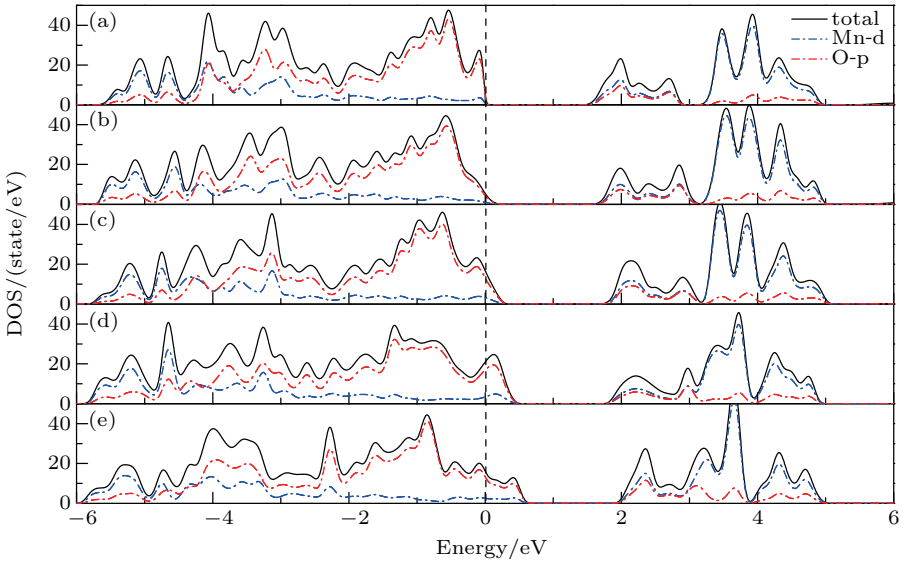


Fig. 3. (color online) Densities of states of (a) Na_2MnO_3, (b) $Na_{1.75}MnO_3$, (c) $Na_{1.5}MnO_3$, (d) $Na_{1.25}MnO_3$, and (e) Na_1MnO_3, respectively. The black, blue, and red lines represent the total densities of states of Na_xMnO_3, partial density of states of Mn-d, and partial density of state of O-p, respectively. The dashed line in the middle represents the Fermi level.

3.4. Diffusion of Na^+ in Na_2MnO_3

Since the mobility of Na-ions is closely related to the rate capability of batteries, we also performed an energy barrier analysis for the process of Na^+ mobility in Na_2MnO_3. There are two main cases of Na^+ migration in Na_2MnO_3: (i) Na^+ migration within the Na layer, and (ii) Na^+ migration between Mn layer and Na layer.

In the case of Na^+ diffusion within the Na layer, the 4h and 2c are the two main sites. Figure 4(a) shows that within this layer, Na^+ migration involves four paths, including two paths for 4h–4h (path I and path II) and two paths for 2c–4h (path III and path IV). As a Na^+ ion diffuses from the 4h to an adjacent 4h site, it can migrate through the octahedral of the O atom along path I with an energy barrier of 0.85 eV, or across the bottom of the 2b site along path II with an energy barrier of 0.89 eV. In addition, as one Na^+ diffuses between the 2c and the adjacent 4h site, it migrates through the octahedral of the O atom along path IV with an energy barrier of 0.99 eV, or across the bottom of the Mn-4g site along path III with an energy barrier of 0.82 eV. The reverse migration processes have almost equal energy barriers due to the similar formation energies of Na_2MnO_3 with a vacancy at the 2c or 4h sites. These barriers are slightly higher than those reported in a previous study on Li migration in Li_2MnO_3,[39] and it is reasonable because the larger ion radius of Na may increase the difficulty of movement of Na compared to Li because of obstruction due to other atoms. In summary, the height of these barriers is different depending on their individual local cation landscapes for the different paths. Path IV exhibits the lowest energy barrier of the four paths within the Na layer. This path is also the lowest energy barrier path for Li migration within the Li-layer in Li_2MnO_3.[39]

Next, we investigate how one Na^+ ion diffuses between the Na layer and the Mn layer by drawing the two main migration paths, in Fig. 4(a), corresponding to the 4h–2b (path V) and the 2c–2b (path VI). In this case, the corresponding energy barriers from the Mn layer to the Na layer, are 1.40 and 1.33 eV for path V and path VI as shown in Fig. 4(b), respectively. However, for the reverse paths from the Na layer to the Mn layer, the energy barriers are much lower at values of 0.91 eV and 0.84 eV for path V and path VI, respectively. The difference between the opposite direction barriers is due to the remarkable difference in the formation energies of Na_2MnO_3 with a vacancy at the 4h and 2b (or 2c) sites. From these energy barrier values, it is possible to determine that Na^+ ions migration from the Na layer to the Mn layer along path VI has the lowest barrier, which is a similar situation to Li migration from the Li layer to the Mn layer in Li_2MnO_3. Moreover, the potential migration of Na^+ between two adjacent 2b sites in the Mn layer was also considered. However, the results indicate that this process is impossible because of the very high energy barrier associated with the MnO_6 octahedral.

Overall, these results imply that the lowest energy barrier (0.82 eV) of the four kinds of Na^+ migration in the Na layer is associated with path IV from the 2c to 4h site, and the lowest energy barrier (0.84 eV) of Na^+ migrations between the Na layer and the Mn layer is associated with path VI from the 2c to 2b site. These results reveal that the Na^+ ions at the 2c site tend to migrate to adjacent 4h or 2b sites, which is consistent with the previous results of Section 3.2, which indicates that Na^+ would be initially de-intercalation from the 2c site during charging. Furthermore, the small difference of the energy barriers of the paths 2c→4h, 4h→2c, 4h→4h, 2c→2b, and 4h→2b indicate that Na^+ can easily backfill empty sites in the Mn layer and Na layer during the discharging process. This phenomenon could lead to an acceptable cycle performance of the battery, which is promising for the prospective future application.

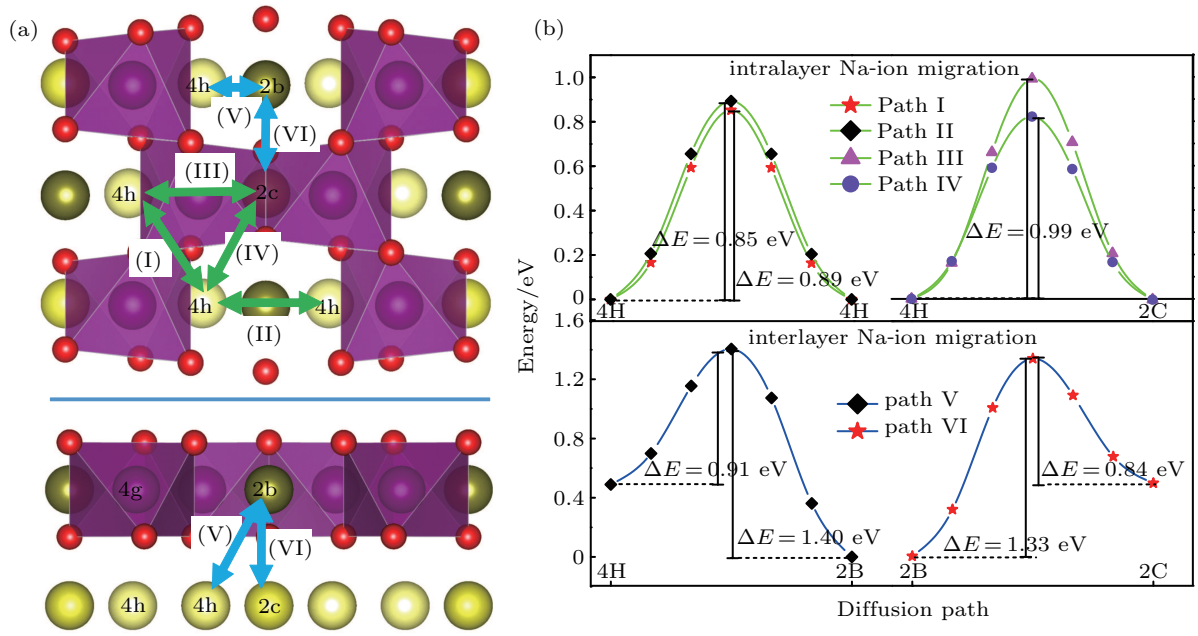


Fig. 4. (color online) (a) The diffusion path of Na^+ in the Na layer (path I–IV, represented by blue arrow) and between Na layer and Mn layer (path V–VI, represented by green arrow); (b) diffusion barrier of Na^+ migration in the Na layer (path I–IV, represented by green line) and between Na layer and Mn layer (path V–VI, represented by blue line).

3.5. Elastic constant of Na_xMnO_3

The elastic constants of materials are closely related to their mechanical properties. In order to investigate the stiffness and stability of Na_2MnO_3 during the charging process, both the elastic constants of Na_2MnO_3 and Li_2MnO_3 were determined using first-principle calculations and the results are shown in Fig. 5(a) and Table S1. From Fig. 5(a), it can be seen that the elastic constants of Na_2MnO_3 are basically the same as Li_2MnO_3 for C_{44}, C_{66}, and only slightly lower than Li_2MnO_3 for C_{11}, C_{22}, C_{33}, and C_{55}, which proves that Na_2MnO_3 has a similar mechanical stiffness and structural stability to Li_2MnO_3.

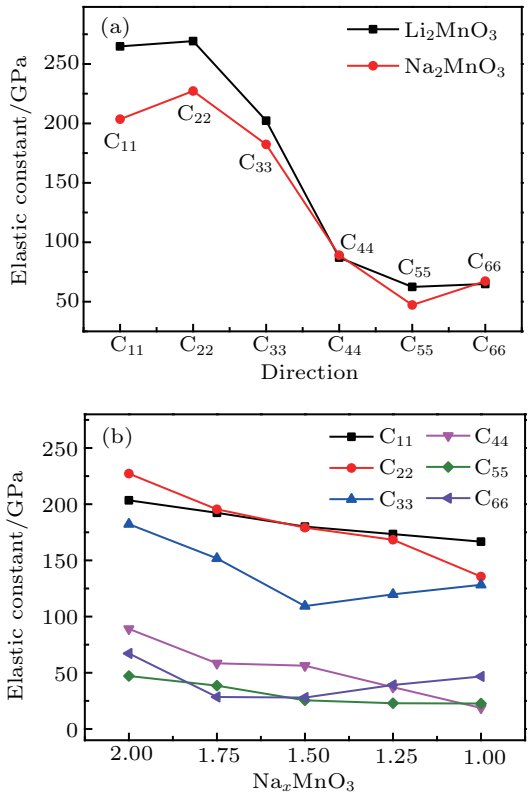


Fig. 5. (color online) (a) Calculated elastic constants (GPa) of Li_2MnO_3 and Na_2MnO_3; (b) calculated elastic constants (GPa) of Na_xMnO_3.

Figure 5(b) shows the detailed elastic constants for Na_xMnO_3 ($x = 1.00$, 1.25, 1.50, 1.75, and 2.00). From these results, it can be determined that the elastic constants C_{11}, C_{22}, C_{44}, and C_{55} decrease slowly with x from 2.00 to 1.00, which is an indication of the favorable stability of Na_xMnO_3. It should be noted that small increases in the elastic constant are observed for C_{33} and C_{66} from $Na_{1.5}MnO_3$ to Na_1MnO_3. However, the trend of the slow decrease remained.

In conclusion, the elastic constants of Na_xMnO_3 decrease slowly during the process of Na^+ de-intercalation, intimating that the mechanical stiffness was well-maintained the departure of Na^+ from Na_xMnO_3. Furthermore, it should be noted that the lowest elastic constants of $NaMnO_3$ in Na_xMnO_3 are still high enough to maintain the structural stability.

4. Conclusions

In this paper, we have reported on a systematic first-principle investigation on the electrochemical redox mechanism of stoichiometric Na_2MnO_3. Through calculations of the phonon spectrum and AIMD simulations, Na_2MnO_3 is proven to be a dynamically stable structure. A comparison of the band structure of Li_2MnO_3 and Na_2MnO_3 revealed that the bandgap of the latter (1.55 eV) is smaller, which indicates that it has a better conductivity than Li_2MnO_3 (1.87 eV). By investigating the Na^+ de-intercalation process from Na_2MnO_3 to $Na_{0.5}MnO_3$, it was determined that Na^+ de-intercalate oc-

curred according to the order 2c, 2b, and 4h, respectively, and a reversible capacity of 269.69 mA·h·g^{-1} was achieved. Using PDOS and Bader atomic charge analysis, the O atom near the vacancy of the de-intercalated Na is shown to be responsible for the charge compensation during the charging process, which is similar to the compensation mechanism for Li_2MnO_3. The mechanism of Na^+ diffusion in Na_2MnO_3 was determined as that of the migration path with the lowest energy barrier of Na_2MnO_3, which is similar to the case of Li migration in Li_2MnO_3. The lowest energy barrier (0.82 eV) of Na^+ migration within the Na layer was along path IV from 2c to 4h site, and the lowest energy barrier (0.84 eV) of Na^+ migration between the Na layer and the Mn layer was along path VI from the 2c to 2b site. It was also determined that the small differences of energy barriers of paths 2c→4h, 4h→2c, 4h→4h, 2c→2b, and 4h→2b indicate that Na^+ can backfill empty sites within the Mn layer and Na layer easily during the discharging process. Furthermore, the slow decrease of the elastic constants indicates a favorable cycle stability. The desirable properties of high capacity, acceptable conductivity, rate capability, and cycle performance demonstrated by in Na_2MnO_3 indicate that it is a very promising cathode material for NIBs. These results lay the foundation for a deeper understanding of the mechanism of the SLOs cathode, which is important in the design of high-performance electrode materials.

References

[1] Idota Y, Kubota T, Matsufuji A, Maekawa Y and Miyasaka T 1997 *Science* **276** 1395
[2] Yoo E, Kim J, Hosono E, Zhou H S, Kudo T and Honma I 2008 *Nano Lett.* **8** 2277
[3] Oyama N, Tatsuma T, Sato T and Sotomura T 1995 *Nature* **373** 598
[4] Ji L, Rao M, Aloni S, Wang L, Cairns E J and Zhang Y 2011 *Energy Environ. Sci.* **4** 5053
[5] Wang Y and Cao G 2008 *Adv. Mater.* **20** 2251
[6] Hannan M, Lipu M, Hussain A and Mohamed A 2017 *Renew. Sust. Energ. Rev.* **78** 834
[7] Horeh N B, Mousavi S and Shojaosadati S 2016 *J. Power Sources* **320** 257
[8] Ling S G, Guo J, Xiao R J and Chen L Q 2016 *Chin. Phys. B* **25** 018208
[9] Slater M D, Kim D, Lee E and Johnson C S 2013 *Adv. Funct. Mater.* **23** 947
[10] Hao H, Liu Z, Zhao F, Geng Y and Sarkis J 2017 *Resour. Policy* **51** 100
[11] Palomares V, Serras P, Villaluenga I, Hueso K B, Carretero-González J and Rojo T 2012 *Energy Environ. Sci.* **5** 5884
[12] Ellis B L and Nazar L F 2012 *Curr. Opin. Solid St. M.* **16** 168
[13] Pan H, Hu Y S and Chen L 2013 *Energy Environ. Sci.* **6** 2338
[14] Wessells C D, Peddada S V, Huggins R A and Cui Y 2011 *Nano Lett.* **11** 5421
[15] Zheng Y, Zhou T, Zhang C, Mao J, Liu H and Guo Z 2016 *Angew. Chem. Int. Ed.* **55** 3408
[16] Xie F, Zhang L, Su D, Jaroniec M and Qiao S Z 2017 *Adv. Mater.* **29** 1700989
[17] Kim S W, Seo D H, Ma X, Ceder G and Kang K 2012 *Adv. Energy Mater.* **2** 710
[18] Berthelot R, Carlier D and Delmas C 2011 *Nat. Mater.* **10** 74
[19] Assadi M and KatayamaYoshida H 2017 *Phys. Chem. Chem. Phys.* **19** 23425
[20] Cao Y, Xiao L, Wang W, Choi D, Nie Z, Yu J, Saraf L V, Yang Z and Liu J 2011 *Adv. Mater.* **23** 3155
[21] Li Y, Feng X, Cui S, Shi Q, Mi L and Chen W 2016 *Cryst. Eng. Comm.* **18** 3136
[22] Ding J J, Zhou Y N, Sun Q and Fu Z W 2012 *Electrochem. Commun.* **22** 85
[23] Yabuuchi N, Kajiyama M, Iwatate J, Nishikawa H, Hitomi S, Okuyama R, Usui R, Yamada Y and Komaba S 2012 *Nat. Mater.* **11** 512
[24] Kee Y, Dimov N, Champet S, Gregory D H and Okada S 2016 *Ionics* **22** 2245
[25] Wang P F, You Y, Yin Y X and Guo Y G 2016 *J. Mater. Chem. A* **4** 17660
[26] Yu H, Guo S, Zhu Y, Ishida M and Zhou H 2014 *Chem. Commun.* **50** 457
[27] Chen H, Hao Q, Zivkovic O, Hautier G, Du L S, Tang Y, Hu Y Y, Ma X, Grey C P and Ceder G 2013 *Chem. Mater.* **25** 2777
[28] Kim D, Lee E, Slater M, Lu W, Rood S and Johnson C S 2012 *Electrochem. Commun.* **18** 66
[29] Mu L Q, Hu Y S and Chen L Q 2015 *Chin. Phys. B* **24** 038202
[30] Li F, Zhu Y E, Sheng J, Yang L, Zhang Y and Zhou Z 2017 *J. Mater. Chem. A* **5** 25276
[31] Yabuuchi N, Takeuchi M, Komaba S, Ichikawa S, Ozaki T and Inamasu T 2016 *Chem. Commun.* **52** 2051
[32] Freire M, Kosova N, Jordy C, Chateigner D, Lebedev O, Maignan A and Pralong V 2016 *Nat. Mater.* **15** 173
[33] McCalla E, Sougrati M T, Rousse G, Berg E J, Abakumov A, Recham N, Ramesha K, Sathiya M, Dominko R and Van Tendeloo G 2015 *J. Am. Chem. Soc.* **137** 4804
[34] McCalla E, Abakumov A M, Saubanère M, Foix D, Berg E J, Rousse G, Doublet M L, Gonbeau D, Novák P and Van Tendeloo G 2015 *Science* **350** 1516
[35] Yu H J, Ishikawa R, So Y G, Shibata N, Kudo T, Zhou H S and Ikuhara Y 2013 *Angew. Chem. Int. Ed.* **52** 5969
[36] Yu H J and Zhou H S 2013 *J. Phys. Chem. Lett.* **4** 1268
[37] Johnson C, Kim J, Lefief C, Li N, Vaughey J and Thackeray M 2004 *Electrochem. Commun.* **6** 1085
[38] Zuo Y, Li B, Jiang N, Chu W, Zhang H, Zou R and Xia D 2018 *Adv. Mater.* **30** 1707255
[39] Xiao R, Li H and Chen L 2012 *Chem. Mater.* **24** 4242
[40] Li B, Yan H, Zuo Y and Xia D 2017 *Chem. Mater.* **29** 2811
[41] Zheng L, Wang H, Luo M, Wang G, Wang Z and Ouyang C 2018 *Solid State Ionics* **320** 210
[42] Kresse G and Furthmüller J 1996 *Comp. Mater. Sci.* **6** 15
[43] Perdew J P, Burke K and Ernzerhof M 1996 *Phys. Rev. Lett.* **77** 3865
[44] Liechtenstein A, Anisimov V and Zaanen J 1995 *Phys. Rev. B* **52** R5467
[45] Togo A and Tanaka I 2015 *Scr. Mater.* **108** 1
[46] Henkelman G, Uberuaga B P and Jónsson H 2000 *J. Chem. Phys.* **113** 9901
[47] Henkelman G, Arnaldsson A and Jónsson H 2006 *Comp. Mater. Sci.* **36** 354
[48] Yang J H, Song S, Du S, Gao H J and Yakobson B I 2017 *J. Phys. Chem. Lett.* **8** 4594
[49] Aydinol M, Kohan A, Ceder G, Cho K and Joannopoulos J 1997 *Phys. Rev. B* **56** 1354
[50] Okamoto Y 2011 *J. Electrochem. Soc.* **159** A152
[51] Koyama Y, Tanaka I, Nagao M and Kanno R 2009 *J. Power Sources* **189** 798